Microsyst Technol (2005) 11: 950–957
DOI 10.1007/s00542-005-0563-z

TECHNICAL PAPER

Jia-Yang Juang · David B. Bogy

Nanotechnology advances and applications in information storage

Received: 8 July 2003 / Accepted: 15 December 2003 / Published online: 18 May 2005

Abstract A brief review of some applications of nanotechnology to information storage is given with the focus on self-assembled nanoporous alumina templates for patterned media.Ordered nanoporous alumina templates were fabricated by self-assembly technology. A two-step anodization process was also carried out to obtain templates with pores perpendicular to the substrate without removing the aluminum and barrier layer. Polycrystalline structure was observed with a grain size of about 2 μm in which the pores were almost perfect hexagonally ordered. The pore arrays exhibit different orientation along the boundaries of neighboring grains. Nanopatterning implemented by electron-beam lithography demonstrates the ability to write pores forming concentric circles with pore diameter as small as 50 nm.

1 Introduction

As the demand on information storage capacity keeps increasing, nanotechnology becomes a viable or even inevitable approach to achieve areal densities of 1 Tb/in^2. Applications of nanotechnology to information storage so far can be divided into three main categories: Nanoscale phenomena in conventional hard disks, probe-based recording, and patterned media magnetic recording.

This study is supported by the Computer Mechanics Laboratory (CML) at University of California, Berkeley. J. Y. Juang has also been supported by The California State Nanotechnology Fellowship.

J.-Y. Juang · D. B. Bogy (✉)
Computer Mechanics Laboratory,
Department of Mechanical Engineering,
University of California Berkeley,
Berkeley, CA 94720, USA
E-mail: dbogy@cml.me.berkeley.edu

With the areal density increasing in current hard disk drives, the physical spacing or flying height (FH) between the transducer housed on an air bearing slider and the disk media must decrease to 3.5 nm for 1 Tb/in^2 areal density (Wood 2000). Zhu and Bogy (2002) developed a slider air bearing surface optimization algorithm, which can obtain optimal slider designs with less than 5 nm FH. In order to achieve a reliable interface, the dynamic issues of slider-disk interface must also be taken into consideration. Thornton and Bogy (2003) proposed an analytical model for understanding the dynamic behavior and instability of ultra-low flying height air bearing sliders in proximity based on nonlinear dynamics.

Instead of using magnetic materials, Vettiger et al. (2002) demonstrated a probe-based thermomechanical data storage system, called "Millipede". The writing process is a combination of applying a local force by the cantilever/tip to the polymer and softening it by heating. The reading is done by detecting the change of resistance as the cantilever/ tip scans across a data bit indentation. Initial areal densities of 100–200 Gb/in^2 have been shown with a 32×32 cantilever array. Millipede shows promises for future storage but there are still several challenges to be overcome, such as the uniformity of cantilever/tip arrays, overall system reliability, and data rates.

The areal density in conventional magnetic storage media, especially for hard disk drives, is expected to reach a physical limitation known as the superparamagnetic limit because of thermal instability. Patterned media has been proposed as one solution to overcome this limitation (Hughes 2001). Unlike current magnetic recording, which uses continuous granular media, patterned media domains are discrete. The bits on the media are physically isolated from their neighbors so magnetic interactions are smaller. One terabit per square inch is potentially achievable with a bit size of around 25 nm.

The fabrication methods of patterned media can be divided into two categories: One uses IC fabrication

techniques, including lithography, magnetic material deposition, and lift-off (Ross et al. 1999). But the bit arrays with sub micron or even tens of nanometer feature sizes are too small to be defined by conventional optical lithography. Advanced non-optical lithography technology, such as electron-beam, imprinting (Wu et al. 1998), X-ray, ion-beam, and interference lithographies, will be required. The main drawback of this approach is that the aspect-ratio of the data bit is limited to be about one.

The other approach used to fabricate patterned media is by self-assembled nanostructures. Semiconductor nanowire arrays, such as silicon and zinc oxide, have been grown by CVD based on the vapor-liquid-solid (VLS) mechanism (Huang et al. 2001). Unfortunately, there is no similar way to grow high-aspect ratio ordered magnetic nanowires. Sun et al. (2000) demonstrated the synthesis of monodisperse iron-platinum (FePt) nanoparticles with tunable diameter from 3 to 10 nm. Another alternative is to use self-assembled nanoporous structures as templates to grow magnetic nanowires within the pores, which has been investigated by several research groups (AlMawlawi 1991; Masuda and Fukuda 1995; Metzger et al. 2000; Nielsch et al. 2000; Tsuya et al. 1987; Zheng et al. 2000). In this paper, we focus on the fabrication of porous alumina templates.

Porous oxide growth with a hexagonal pore arrangement on aluminum under anodic bias in various dilute acids has been studied for more than 40 years (Keller et al. 1953; O'Sullivan and Wood 1970). Figure 1 shows the hexagonally ordered pore arrangement.

However, the underlying pore arrangement mechanism is still not well understood. One likely explanation is that, due to the expansion of the aluminum during the anodization, the alumina, which is inherently porous, will form a structure with minimum energy. The hexagonal honeycomb structure is one of the close-packed, robust, and minimum energy forming structures found in nature, and it is expected to be obtained after the anodization of an aluminum foil with a smooth surface under proper anodization conditions. Straight alumina channels are formed as the aluminum ions diffuse out of, and oxygen ions diffuse into, the barrier layer under the electric field. Dissolution of the alumina takes place more readily at concave sites due to the concentrated electric field. Thamida and Chang (2002) used linear stability theory and a weakly nonlinear evolution equation to predict the transition from porous to non-porous alumina at a pH equal to 1.77. Broughton and Davies (1995) produced a stochastic simulation model, which was used to predict an anodic oxide membrane formation. Jessensky et al. (2001) proposed the idea that the resulting mechanical stress, caused by the volume expansion of the aluminum at the metal and oxide interface, promotes the formation of ordered hexagonal pore arrays. Zhang et al. (1998) proposed a cellular growth mechanism in ordered porous alumina due to oxide propagation at a curved metal-oxide interface.

Prepatterning on the aluminum surface with particular features prior to the anodization process has been successfully used to guide the growth of straight pores. Li et al. (2000) prepared hexagonally ordered pore array structures with variable interpore distance based on prepatterning by electron-beam lithography and a subsequent anodization in oxalic acid solution. Liu et al. (2001) also obtained similar results by prepatterning with focused ion beam lithography. Masuda et al. (2001) even fabricated a pore array with square or triangular openings based on the two-dimensional tiling of the cell configuration of anodic porous alumina. They also showed that the shapes of the cells and openings were determined not by the shape of the depressions which served as the initiation sites for pore growth but by the arrangement of the initiation sites in two-dimensional space on the aluminum surface.

Regularity of the pore arrangement in porous alumina can be increased by increasing the anodizing time under proper conditions. However, the template obtained by prolonged anodization is not suitable for patterned media applications because of the excessive thickness and irregular pore configuration on the top surface. Masuda and Satoh (1996) presented a two-step anodizing process to fabricate ordered through-channel arrays with tunable thickness.

To our knowledge, a concentric circular pore arrangement in alumina has not been shown, but this could be very useful for the magnetic patterned media application. In our study, electron-beam lithography was used as the means to produce the concentric circular features.

2 Experimental setup and procedure

2.1 Self-assembled nanoporous templates

Several similar recipes, with minor differences, for preparing anodic alumina porous templates can be found in

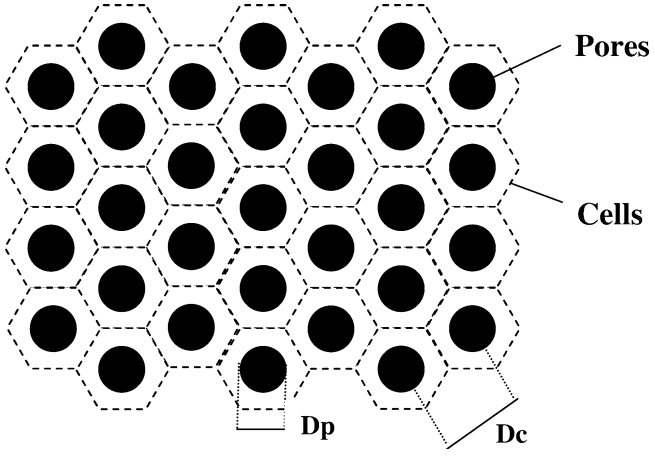

Fig. 1 Ideal hexagonal cell arrangement of a porous alumina template

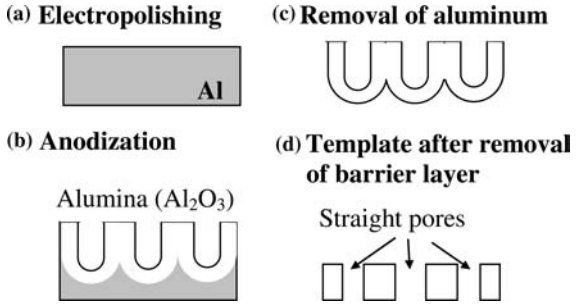

Fig. 2 Schematic process flow of nanoporous templates

the literature. The approach used by Keller et al (1953), O'Sullivan and Wood (1970), and Masuda and Fukuda (1995) was adopted in this research.

Figure 2 illustrates the scheme of the process for the preparation of self-assembled nanoporous templates. High purity (99.999%) aluminum foils purchased from Goodfellow were used as substrates. After the foil was carefully ultrasonically cleaned and degreased by acetone, it was then electropolished to lower the roughness of the aluminum surface. The electropolishing was conducted under a constant voltage of 3.5 V at room temperature for 10 min in a mixture of 60 wt % perchloric acid and ethanol ($HClO_4$: C_2H_5OH = 1: 4 by volume) with aluminum as the anode and copper plate as the cathode. Anodization was performed in 0.3 M aqueous oxalic acid at 40 V and 25°C for 2 h. Anodization is usually carried out at a high voltage in dilute acids at lower temperature in order to promote the growth of larger cells and pores. After anodization, the alumina foil was dipped into a saturated $HgCl_2$ solution to remove the aluminum and keep the porous alumina unharmed. Subsequent etching treatment was conducted in a 5% wt H_3PO_4 solution at 25°C to remove the barrier layer and, hence, reveal the pores. This helps us to observe the pore arrangement at the bottom of the templates.

Figure 3 illustrates a two-step anodization process in which the hexagonally ordered pore configuration can be achieved without removal of the barrier. The detailed process sequence is described as follows. The aluminum foil was degreased with acetone. The first anodization

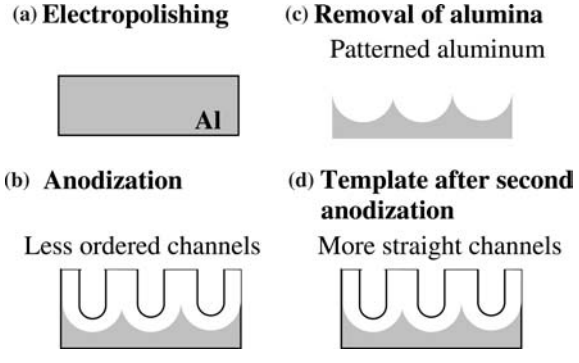

Fig. 3 Schematic process flow of a two-step anodization process for nanoporous templates

was conducted at a constant voltage of 40 V in a 0.4 M aqueous oxalic acid at 25°C for 18 h. This alumina was then stripped away by a mixture of H_3PO_4 (6 wt%) and H_2CrO_4 (1.8 wt%) at 60°C. The remaining periodic concave patterns on the aluminum foil acted as self-assembled masks for the second anodization in which all conditions were the same as those in the first one.

2.2 Nanopatterning

In this study nanopatterning was implemented by use of the Nanometer Pattern Generation System based on electron-beam lithography.

Electron-beam lithography or EBL is a high-resolution patterning technology in which high-energy electrons are focused into a narrow beam and are used to expose electron-sensitive resists point-by-point. Unlike optical lithography, the resolution of EBL is limited by proximity effects. This refers to the tendency of scattered electrons to expose nearby areas that may not be intended for exposure. The scattering can be divided into forward and backscatter. Forward scatter occurs over a small range of angles with respect to the incident beam and leads to a slight broadening of the image. Backscatter contributes a large fog area of exposure. Commercially available EBL systems are now capable of routinely writing features with resolutions of tens of nanometers. More details on EBL can be found in Campbell (1996) and Rai-Choudhury (1997).

"Nanometer Pattern Generation System" or NPGS is an integrated software program for the delineation of complex structures using a commercial electron beam microscope. Patterns are created using Design-CAD, which is a commercial computer-aided-design program.

3 Results and discussions

Scanning electron microscopy (SEM) and atomic force microscopy (AFM) were used to measure the topography of the samples made in this study. Figure 4 a shows the SEM image of the raw aluminum foil. The stripes on the surface are a result of the manufacturing process. AFM study shows that the root-mean-square (rms) roughness is 37.84 nm over a 3×3 um area. The roughness is expected to be even larger over a broader area. After the electropolishing treatment, the rms roughness was lowered to 0.731 nm over a 1 μm square area. Figure 4b shows the SEM image of an electropolished aluminum foil. The surface topographies of the porous alumina templates without and with electropolish are shown in Fig. 5. Comparing Fig. 4a with Fig. 5a, we find that the pores tend to form along the stripes, which reinforces the suggestion made in the previous section. The pore arrangement was more random on the electropolished foils, which indicates the pores grew randomly in the very beginning of the anodizaton process.

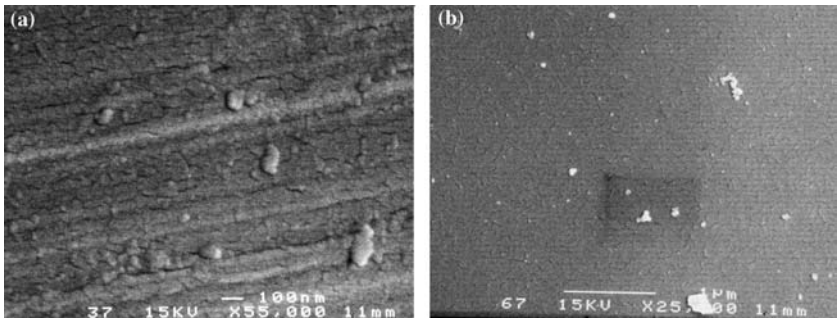

Fig. 4 a SEM image of a raw aluminum foil, 55,000 X. b Electropolished, 25,000 X, 10 min, ~ 3.5V, room temperature

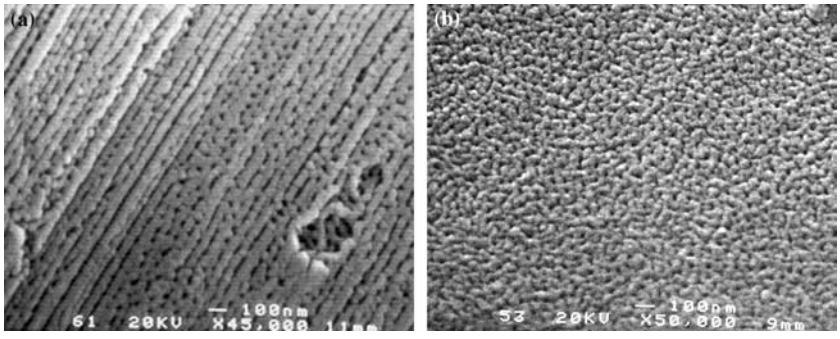

Fig. 5 a SEM top view of a porous alumina template at 45,000 X, degreased with acetone, anodized in oxalic acid for 2 h 38 mins at 27°C, non-electropolished; b Anodized, ×50,000, 0.3 M oxalic acid, 4 h, 40 V, ~7°C, electropolished

Figure 6 shows an SEM dissected view of the template before the removal of the barrier layer and Figs. 5a, 7, 8, and 9 show the enlargement of each image.

The fabrication was conducted with a two-hour anodization according to the process described in Sect. 2.1. The top and bottom views illustrate the pore configurations in the earlier and later anodization stages, respectively. A polycrystalline convex feature arrangement with domains of about 2 μm is observed on the bottom view as shown in Fig. 7. Within each domain, almost perfect hexagonally arranged convex features are observed. In the domains, each hemisphere is surrounded by six others hexagonally, which are interconnected to form a network structure. The cell size or the center-to-center distance between neighboring hemispheres is about 100 nm, which is consistent with the results obtained by other researchers. This cell size is tunable and is believed to be proportional to the anodizing voltage.

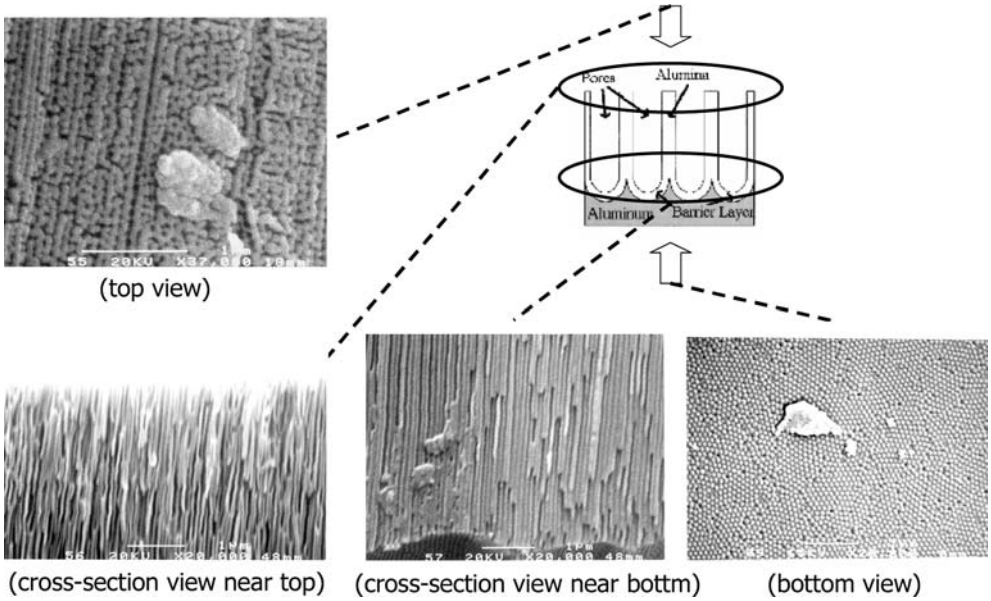

Fig. 6 Top, cross-section, and bottom view of the alumina template. The anodization was carried out according to process described in Sect. 2.1

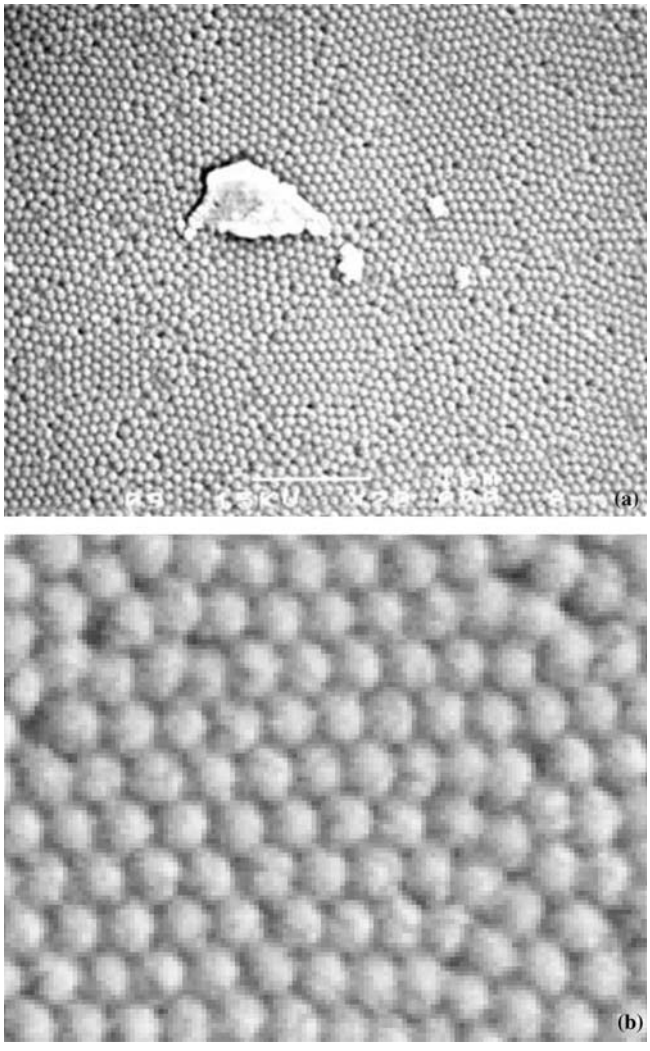

Fig. 7 a An SEM enlargement of bottom view of the template shows the polycrystalline arrangement of convex arrays before the removal of barrier layer. b A SEM enlargement of one domain of the template shows the almost perfect hexagonally ordered convex features. The cell size is about 100 nm

More details can be found in the literature (Keller et al. 1953; O'Sullivan and Wood 1970; Wehrspohn et al. 2000).

A transition of pore growth from a crooked to a straight pattern can be observed from the cross sections of the templates in Figs. 8 and 9. An additional barrier layer removal and pore-widening etching process was carried out in 5 wt% phosphoric acid at 25°C for 1.5 h. The porous template obtained is shown in Fig. 10. The pore arrangement is similar to that before removal of the barrier layer. The reason the pores are not as ordered as the hemispheres is probably due to the over-etching in the pore-widening process.

Figure 11 shows the "top-view" SEM image of the alumina grown by a two-step anodization. Although the pores are not as clear as those in Fig. 10, which was done by a one-step anodization and removal of the barrier layer, the pore arrangement as well as cell size resembles that in Fig. 10.

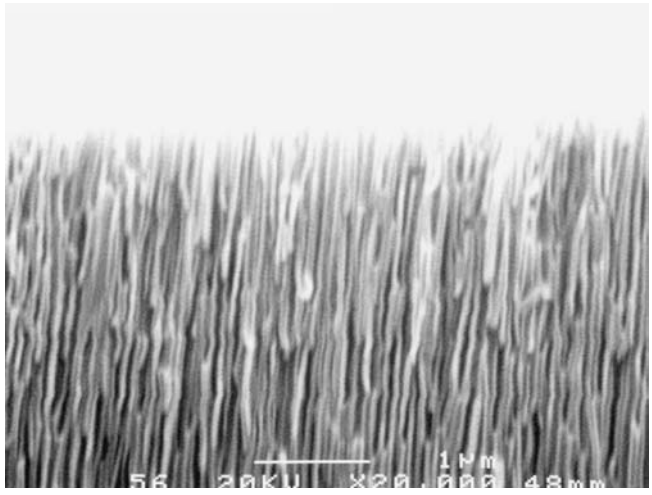

Fig. 8 An SEM enlargement of near-top cross section of the template shows the irregular pores, which were formed in the earlier stage of anodization

In order to look into the feasibility of "guided self-assembly" of porous templates with concentric circular pore arrangements, NPGS accompanied with a scanning electron microscope (JEOL 6400) has been used to write various prepatterns with sub-micrometer scale features. The substrate was a silicon wafer with a one um electron-beam evaporated pure aluminum film. The detailed procedure of pattern writing on polymers is described as follows. A positive poly(methyl methacrylate) (PMMA) electron-sensitive resist with a molecular weight of 950,000 3% in chlorobenzene was spun at 500 rpm for 3 s then 4,000 rpm for 20 s onto the substrate to achieve a thickness of about 150 nm. Then it was baked 2 h at 160°C. After that the patterns were written on the

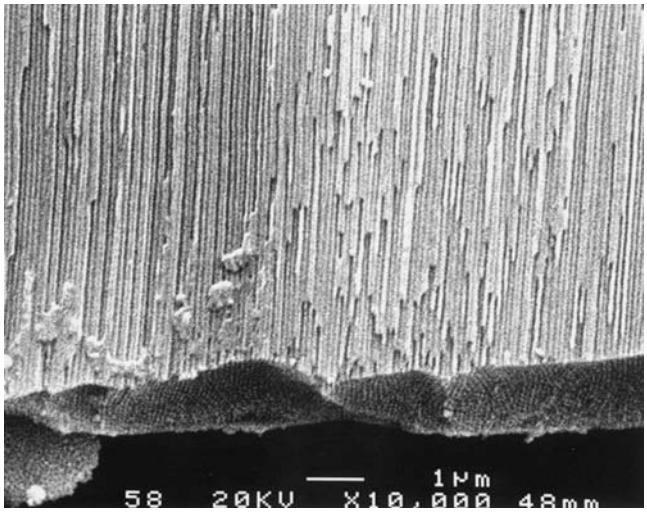

Fig. 9 An SEM enlargement of near-bottom cross section of the template shows the straight pores, which were formed in the later stage of anodization. The *bottom* surface is the barrier layer

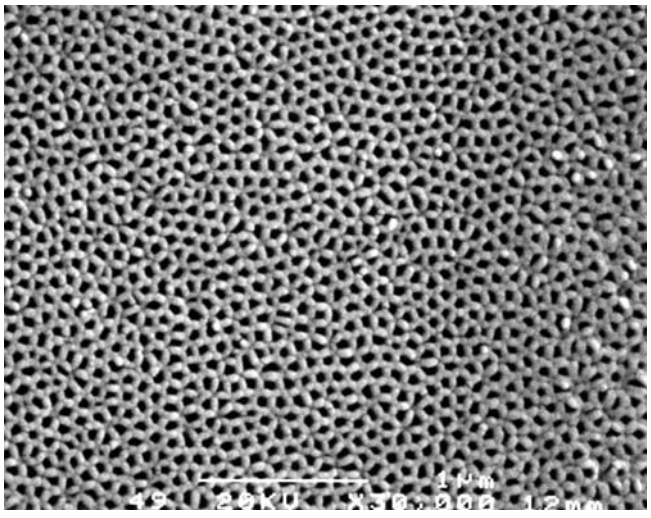

Fig. 10 An SEM of the bottom-view of the alumina template by single-step anodization. It was anodized in oxalic acid for about 23 h and was then dipped in a saturated $HgCl_2$ solution for about 1.5 h. The barrier layer was removed in 5% H_3PO_4 for 1.5 h

PMMA at 35 kV. The exposed wafers were developed in 3:1 IPA (Isopropyl Alcohol = 2 Propanol): MIBK (Methl Isobutyl Ketone = 2-Pentanone, 4-methyl) at 25°C for 70 s. The wafers were then immediately rinsed in IPA for about 20 s, followed by DI water for about 20 s, and then they were blown dry with a clean gas. Figure 12 shows the pores on PMMA, forming concentric circles with radii from 70 μm to 180 μm. The diameters of the pores are about 100 nm in Fig. 12 a, b, and 50 nm in Fig. 12c. The spacing between any two adjacent circles is 400 nm.

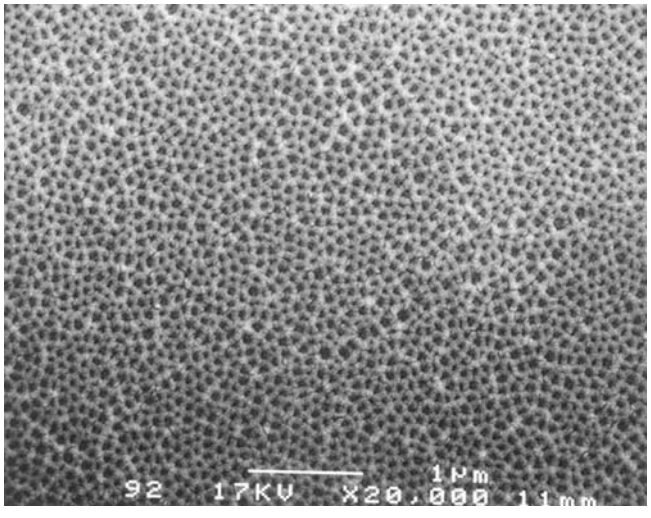

Fig. 11 An SEM of the "top-view" of the alumina template by two-step anodization. Note that the cell size and pore arrangement resemble those of "bottom-view" of the alumina template by single-step anodization

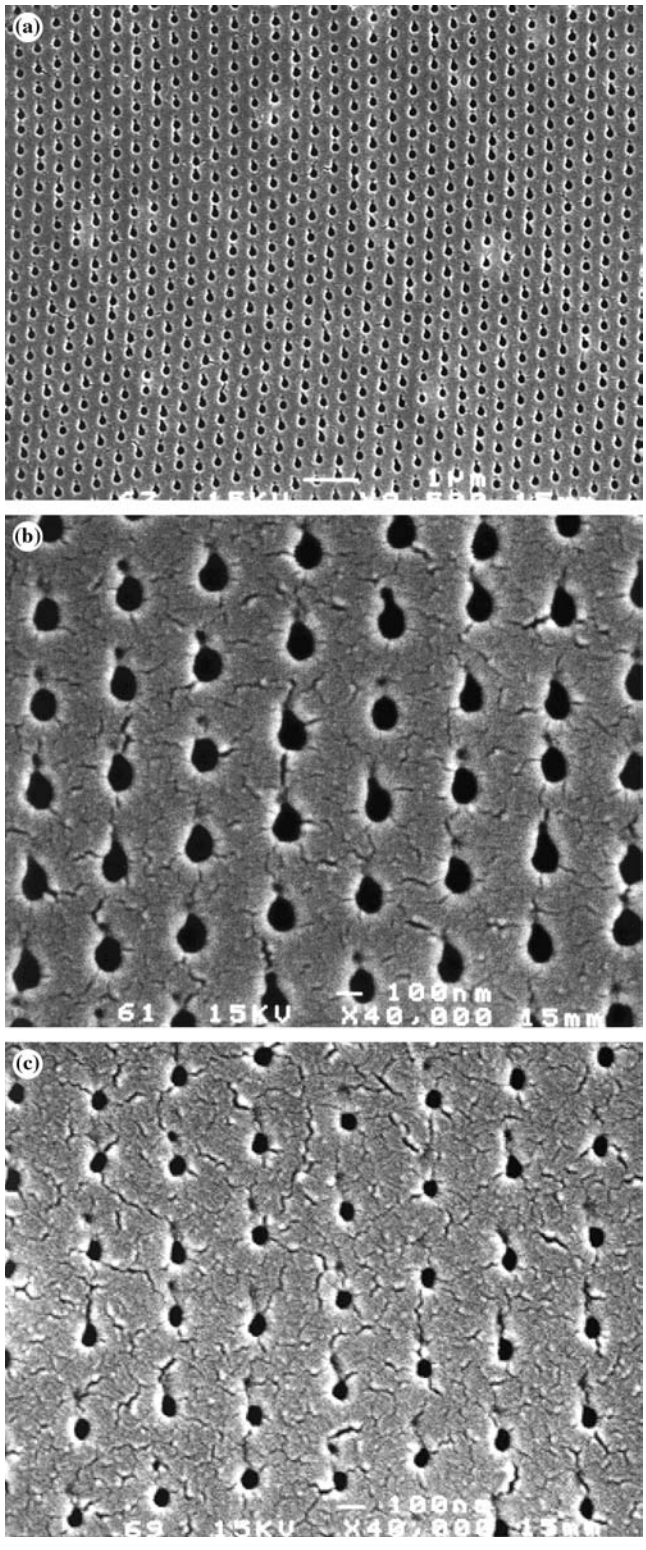

Fig. 12 a Electron-beam written pores on PMMA, forming concentric circles with radii from 70 μm to 180 μm. The EBL parameters were: accelerating voltage 35 kV, beam current 500 pA, center-to-center exposure 400 nm, and exposure time 300 μs; **b** An enlargement of the features in **(a)**; **c** Pores written by electron-beam lithography with the same parameters as those in (a) except the exposure time 200 μs

4 Conclusions and future work

A brief review of nanotechnology advances in information storage, including nanoscale phenomena in conventional hard disks, probe-based recording, and patterned media magnetic recording, is given with the focus on self-assembled nanoporous alumina templates for patterned media.

Self-assembled nanoporous alumina templates have been fabricated. The interpore distance or cell size is 100 nm, which results in an areal pore density of 64.5 Gigabit per square inch. However, the potential of decreasing the interpore distance to 25 nm provides a promise of ultrahigh areal density up to one Terabit per square inch. The main strengths of this approach include: (a) Relatively easy to implement and cost-effective; (b) The potential to achieve ultrahigh areal density with ordered structures; (c) The interpore distance and pore diameter can be arbitrarily tuned simply by choosing an adequate electrolyte as well as controlling the anodizing voltage and the etching time, respectively.

The main drawbacks are: (a) The self-assembled pore configuration is inherently hexagonally ordered and cannot be designed arbitrarily; (b) Advanced lithography techniques may be required to prepattern the aluminum in order to guide the self-assembly of pore formation; (c) The self-assembly process is not a standard silicon one and more effort is required to integrate it into IC compatible and/ or hard disk drive facilities; (d) In the application of patterned media recording, deposition of high quality magnetic materials into the pores needs more emphases. Electroplated magnetic materials may not be a good candidate of high quality recording media.

A two-step anodization process was used to obtain straight through-channels. Self-assembled hexagonally ordered pores were formed after a certain time of anodization. The irregular alumina was then stripped away, leaving the aluminum with ordered pits on the top surface. A second anodization was then carried out with the help of the ordered pits as a mask. Almost perfect ordered pore arrays were observed within domains of 2 μm.

The results of electron-beam lithography demonstrates the ability to write pores arranged in concentric circles with pore diameter less than 50 nm. In the future, we will investigate the feasibility of guided-self-assembly to form templates with concentric circular pore arrangements and the applications for information storage.

Acknowledgements The first author thanks Stanley Kon for helpful discussions on the anodization experimental setup, Ron Wilson for taking SEM images, and Microlab at UC Berkeley for providing facilities.

References

AlMawlawi D, Coombs N, Moskovits M (1991) Magnetic properties of Fe deposited into anodic aluminum oxide pores as a function of particle size. J App Phys 70:4421–4425

Broughton J, Davies GA (1995) Porous cellular ceramic membranes: a stochastic model to describe the structure of an anodic oxide membrane. J Membrane Sci 106:89–101

Campbell SA (1996) The science and engineering of microelectronic fabrication. Oxford University Press

Huang MH, Mao S, Feick H, Yan H, Wu Y, Kind H, Weber E, Russo R, Yang P (2001) Room-temperature ultraviolet nanowire nanolasers. Science 292:1877

Hughes GF (2001) Patterned media''. In: Plumer M, van Ek J, Weller D (eds) The physics of ultra-high-density magnetic recording. Springer, Berlin Heidelberg New York

Jessensky O, Muller F, Gosele U (2001) Self-organized formation of hexagonal pore arrays in anodic alumina. Appl Phys Lett 72:1173–1175

Keller F, Hunter MS, Robinson DL (1953) Structural features of oxide coatings on aluminum. J the Electrochem Soc 100:411–419

Li AP, Muller F, Gosele U (2000) Polycrystalline and monocrystalline pore arrays with large interpore distance in anodic alumina. Electrochem Solid State Lett 3:131–134

Liu CY, Datta A, Wang YL (2001) Ordered anodic alumina nanochannels on focused-ion-beam-prepatterned aluminum surfaces. Appl Phys Lett 78:120–122

Masuda H, Fukuda K (1995) Ordered metal nanohole arrays made by a two-step replication of honeycomb structures of anodic alumina. Science 268:1466–1468

Masuda H, Satoh M (1996) Fabrication of gold nanodot array using anodic porous alumina as an evaporation mask. part 2. Jpn J Appl Phys 35:L126–L129

Masuda H, Asoh H, Watanabe M, Nishio K, Nakao M, Tamamura T (2001) Square and triangular nanohole array architectures in anodic alumina. Adv Mater 13:189–192

Masuda H, Yotsuya M, Asano M, Nishio K, Nakao M, Yokoo A, Tamamura T (2001) Self-repair of ordered pattern of nanometer dimensions based on self-compensation properties of anodic porous alumina. Appl Phys Lett 78:826–828

Metzger RM, Konovalov VV, Sun M, Xu T, Zangari G, Xu B, Benakli M, Doyle WD (2000) Magnetic nanowires in hexagonally ordered pores of alumina. IEEE Trans Magn 36:30–35

Nielsch K, Muller F, Li AP, Gosele U (2000) Uniform nickel deposition into ordered alumina pores by pulsed electrodepostion. Adv Mater 12:582–586

Nielsch K, Muller F, Liu G, Wehrspohn RB, Gosele U, Fischer SF, Kronmuller H (2000) Magnetic nanowire arrays obtained by electro-deposition in ordered alumina templates. In: Electrochemical Processing in ULSI Fabrication III, Andricacos PC, Searson PC, Reidsema-Simpson C, Allongue P, Stickney JL, Oleszek GM (eds) PV-2000-8, Electrochemical Society, Pennington

O'Sullivan, Wood GC (1970) The morphology and mechanism of formation of porous anodic films on aluminum. In: Proceedings of the Royal Society of London 317:511–543

Rai-Choudhury P (ed) (1997) Handbook of microlithography, micromaching, and microfabrication, vol. 1, microlithography. SPIE Optical Engineering Press, Bellingham, Institution of Electrical Engineers, London

Ross CA, Smith HI, Savas TA, Schattenburg M, Farhoud M, Hwang M, Walsh M (1999) Fabrication of patterned media for high density magnetic storage. J Vac Sci Technol B17:3168–3176

Sun S, Murray CB, Weller D, Folks L, Moser A (2000) Monodisperse FePt nanoparticles and ferromagnetic FePt nanocrystal superlattices. Science 287:1989–1992

Thamida SK, Chang HC (2002) Nanoscale pore formation dynamics during aluminum anodization. Chaos 12:240–251

Thornton BH, Bogy DB (2003) Non-linear aspects of air bearing modeling and dynamic spacing modulation in sub 5nm air bearings for hard disk drives. IEEE Trans Magn 39(2):722–728

Tsuya N, Tokushima T, Shiraki M, Wakui Y, Umehara Y, Saito Y, Nakamura H, Katsumata Y, Iwasaki S, Nakamura Y (1987) Magnetic discs using anodic oxidized aluminum substrates. IEEE Trans Magn MAG-23:2242–2244

Vettiger P, Cross G, Despont M, Drechsler U, Dürig U, Gotsmann B, Häberle W, Lantz MA, Rothuizen HE, Stutz R, Binnig GK (2002) The Millipede – nanotechnology entering data storage. IEEE Trans Nanotechnol 1(1):39–55

Wehrspohn RB, Li AP, Nielsch K, Muller F, Erfurth W, Gosele U (2000) Highly ordered alumina films: pore growth and applications. In: Oxide Films, Hebert KR, Lillard RS, Mac Dougall (eds) PV-2000–4. Electrochemical Society, Pennington

Wood R (2000) The feasibility of magnetic recording at 1 tearbit per square inch. IEEE Trans Magn 36:36–42

Wu W, Cui B, Sun XY, Zhang W, Zhuang L, Kong L, Chou SY (1998) Large area high density quantized magnetic disks fabricated using nanoimprint lithography. J Vac Sci Technol B 16:3825–3829

Zhang L, Cho HS, Li F, Metzger RM, Doyle WD (1998) Cellular growth of highly ordered porous anodic films on aluminum. J Mater Sci Lett 17:291–294

Zheng M, Menon L, Zeng H, Liu Y, Bandyopadhyay S, Kirby RD, Sellmyer DJ (2000) Magnetic properties of Ni nanowires in self-assembled arrays. Phys Rev B 62:12282–12286

Zhu H, Bogy DB (2002) Direct algorithm and its application to slider air bearing surface optimization. IEEE Trans Magn 38(5):2168–2170